Soils and Foundations 2016;56(1):19–32

HOSTED BY

ELSEVIER

The Japanese Geotechnical Society

Soils and Foundations

www.sciencedirect.com
journal homepage: www.elsevier.com/locate/sandf

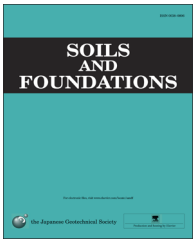

Seismic evaluation of existing arch dams and massed foundation effects

Hasan Mirzabozorg*, Mehdi Varmazyari, Saeed Asil Gharehbaghi

Department of Civil Engineering, KN Toosi University of Technology, 15875-4416 Tehran, Iran

Received 9 September 2014; received in revised form 28 July 2015; accepted 16 September 2015
Available online 15 February 2016

Abstract

In the present paper, the effects of a massed foundation on the nonlinear seismic response of an existing arch dam are investigated. A co-axial rotating smeared crack approach was used to model the nonlinear behavior of the mass concrete in a 3D space which is able to model cracking/crushing under static and dynamic conditions. The analysis also considered the opening/slipping of joints. The reservoir was assumed to be compressible and was modeled using the finite element method with the appropriate boundary conditions. The Dez arch dam was selected for the case study and excited by a maximum credible earthquake. It was found that assuming a massless foundation leads to the overestimation of the stresses within the dam body and causes many more crack profiles than the massed foundation model. As a result, in the case of a massed foundation, no numerical instability was found to exist during the analysis.

Keywords: Arch dams; Dam–reservoir–foundation interaction; Massed foundation; Seismic analysis; Smeared crack model

1. Introduction

Estimating the structural response of existing dams is a major task in dam engineering. To evaluate the seismic safety of arch dams, a 3D dynamic analysis of a dam–reservoir–foundation system, that can consider the following phenomena, is required: (1) dam–foundation interaction, (2) nonlinearities originating from the opening/slipping of the vertical contraction joints and the cracking/crushing of the mass concrete, (3) application of boundary conditions as close as possible to those of the real ones, and (4) application of eligible earthquake records for analyzing the arch dam located in a region with significant seismicity. Several researchers have studied the linear response of arch dams by ignoring the foundation inertia (Lau et al., 1998; Mojtahedi and Fenves, 2000; USACE, 2003; Alves, 2004). Hall (1998) proposed a simple smeared crack model to simulate the contraction and construction joints in the dynamic analysis of arch dams by assuming the flexibility of the foundation rock. At the same time, USBR (1998) evaluated the seismic safety of the Hoover Dam, a high curved arch gravity dam, by assuming a massless foundation. Due to the overestimated results of the conducted analysis, however, an investigation considering the dam–foundation interaction was conducted (USBR, 2002). The results showed that for the model with only foundation-rock flexibility, the stresses were overestimated three times in comparison to those obtained from the model with the massed foundation.

The EACD-3D computer program, originally developed by Fok et al. (1986), employs an analytical procedure for the three-dimensional seismic analysis of concrete dams including the effects of the dam–water interaction and the flexibility of

*Corresponding author. Tel.: +98 21 88779473 5; fax: +98 21 88779475.
E-mail addresses: mirzabozorg@kntu.ac.ir (H. Mirzabozorg), mvarmazyar@dena.kntu.ac.ir (M. Varmazyari), Asil@kntu.ac.ir (S.A. Gharehbaghi).
Peer review under responsibility of The Japanese Geotechnical Society.

http://dx.doi.org/10.1016/j.sandf.2016.01.002

the foundation rock. In EACD-3D-96, the seismic analysis procedure is extended to include the inertia effect and radiation damping arising from the mass of the foundation rock (Tan and Chopra, 1996). The analytical procedure underlying the program just considers the linear behavior of the dam body and the surrounding rock. Thus, the potential for concrete cracking/crushing and for the opening/slipping of the contraction joints during vibrations are not considered. In Wang and Chopra (2008), the analysis procedure of the earlier EACD-3D-96 is extended to consider the spatially varying excitation phenomenon along the dam–foundation rock interface.

Sevim et al. (2012) studied the earthquake behavior of an arch dam using vibration test results assuming a massless foundation. According to the results, very small damping ratio values with the massless foundation model in a seismic analysis lead to an upper-bound estimation of seismically induced stresses. Chopra (2012) investigated the appropriate procedures by studying the factors necessary for estimating the seismic demands on concrete arch dams.

Other researchers have studied the effects of foundation interaction on the seismic response of concrete dams (Mirzabozorg et al., 2003a, 2010a; Noorzad et al., 2007). Ghaemian et al. (2005) studied the effects of foundation shape and mass on the linear seismic response of arch dams using the finite element method including the structure–reservoir interaction. Mirzabozorg et al. (2007) studied the seismic analysis of concrete dams in a 3D space using the smeared crack approach. Wang et al. (2012) investigated the nonlinear seismic behavior of a high arch dam–water–foundation rock system. Hariri-Ardebili and Mirzabozorg (2012) considered the seismic evaluation of concrete arch dams by assuming a massless foundation. They modeled the joints and material nonlinearly and separately. However, not much work has been conducted that considers the effects of massed foundations and the nonlinearities that originate from the contraction/perimetral joints and the mass concrete on the seismic response of arch dams.

Mirzabozorg et al. (2010b) studied the nonlinear seismic response of arch dams considering the massed foundation effect. Berrabah et al. (2012) addressed the effect of the surrounding soil on the linear seismic response of a concrete gravity-arch dam and found that modeling the massed foundation leads to more conservative results. Nevertheless, based on the authors' experience, the conclusions presented in that work are questionable. Hariri-Ardebili and Saouma (2013b) investigated the effects of near-fault vs. far-field ground motions on the linear seismic behavior of a concrete arch dam and found that modeling the massed foundation leads to lower stress levels within the dam body in each case.

Mirzabozorg et al. (2012) considered the linear and nonlinear behaviors of the coupled system of a reservoir–dam–foundation in a 3D space under various conditions of the foundation. They found that a massless foundation overestimates the response of the system. Hariri-Ardebili and Mirzabozorg (2013a) presented a comprehensive study on the seismic behavior of a high arch dam including a massed foundation, the application of infinite elements, and absorbing boundaries on the far-end nodes of the foundation. In that work, the nonlinear behavior was simulated using the proposed smeared crack approach by the first author. It was found that a massed foundation leads to fewer cracks through the dam body. However, joint nonlinearity and compression crushing were not considered in that study.

In the present paper, the effects of a massed foundation on the nonlinear seismic response of an existing arch dam in a 3D space are investigated. The reservoir–structure interaction is taken into account by the finite element method. The nonlinearity originating from the mass concrete is modeled with a co-axial smeared crack approach. The reservoir is assumed to be compressible, and the opening/slipping of the vertical and perimetral contraction joints is included in the analysis. Finally, the viscous condition at the far-end boundary of the foundation is used to model the radiation effect. It is worth mentioning that the main novelty of the present investigation, with respect to previous works by the same authors, is that it takes into account the effects of a massed foundation in addition to both the joint and the material nonlinearity, which have an important impact on the structural response of high slender arch dams. As is known in the field of dam engineering, the common approach to designing new dams or to evaluating existing ones is to assume the massless condition of the foundation rock surrounding the dam due to the conservative results and because of some uncertainties encountered when taking into account the mass effect of the rock. However, having mass effects can lead to lower stress levels, and consequently, lower costs for the required retrofitting works on the dams which are infra-structures with significant impacts on socio-economical aspects. In the present study, it is shown that assuming a massed foundation, which is the real state in nature, leads to more realistic results in a seismic safety evaluation, which is in contrast to the conclusion drawn from the traditional assumption in which foundation flexibility is considered.

2. Foundation interaction and wave propagation

The equations governing P and S wave propagations within the massed foundation rock are

$$\frac{\partial^2 u}{\partial t^2} = V_p^2 \nabla^2 u \tag{1}$$

$$\frac{\partial^2 v}{\partial t^2} = V_s^2 \nabla^2 v \tag{2}$$

$$\frac{\partial^2 w}{\partial t^2} = V_s^2 \nabla^2 w \tag{3}$$

in which, u, v, and w are displacements in the direction of the wave propagation and the other two orthogonal directions, respectively, and V_p and V_s are primary and secondary wave propagation velocities within the rock medium, respectively, derived as

$$V_p = \sqrt{\frac{E_r(1-\upsilon_r)}{\rho_r(1+\upsilon_r)(1-2\upsilon_r)}} \tag{4}$$

$$V_s = \sqrt{\frac{G_r}{\rho_r}} = \sqrt{\frac{E_r}{2(1+\upsilon_r)\rho_r}} \tag{5}$$

where E, G, υ, and ρ are the modulus of elasticity, the shear modulus, Poisson's ratio, and density, respectively, and subscript r indicates that the parameters are pertinent to the foundation rock.

One of the main aspects in seismic loading and wave propagation within a semi-infinite medium, such as the rock underlying structures, is the prevention of the wave reflection from the artificial boundary on the far-end nodes into the provided finite element model. In this study, an appropriate viscous boundary, which is a non-consistent boundary (sometimes called the local boundary), is applied on the far-end boundary of the foundation in a 3D space (Lysmer and Kuhlemeyer, 1969).

$$\sigma = a\rho_r V_P \dot{u} \tag{6}$$

$$\tau_1 = b\rho_r V_S \dot{v} \tag{7}$$

$$\tau_2 = b\rho_r V_S \dot{w} \tag{8}$$

where σ, τ_1, and τ_2 are the normal and two in-plane shear stresses in the global directions, respectively, and u, v, and w are the normal and two tangential displacements, respectively. Based on the discussion reported in Azmi and Paultre (2002), it is found that in applying the three boundary conditions stated in Eqs. (6)–(8), taking the two dimensionless parameters, a, and b, as equal to unity, can lead to more efficiency in absorbing the outgoing seismic waves.

Radiation damping, derived from Eqs. (6)–(8) and applied on the far-end boundary of the foundation, is made up of dashpots that are added to the global damping matrix of the structure, $[C]$. In the present research, these lumped dashpots are determined as

$$C_{11}^i = V_P \rho_r \int_{A_e} N_i dA \tag{9}$$

$$C_{22}^i = V_S \rho_r \int_{A_e} N_i dA \tag{10}$$

$$C_{33}^i = V_S \rho_r \int_{A_e} N_i dA \tag{11}$$

where C_{11}^i, C_{22}^i, and C_{33}^i are the components of lumped damping applied on the ith node of the surface element on the far-end boundary of the surrounding rock in normal and two orthogonal tangential directions, respectively, N_i is the ith node shape function, and all integrations are applied over the area of the considered surface of element A_e.

3. Contraction and perimetral joints

In the present study, a special contact element is used to model the contraction and perimetral joints. The element is able to model the contact between the two adjacent nodes in the 3D domain. This contact element supports compression in the normal direction and shears in the two orthogonal tangential directions. Fig. 1 presents a flowchart used to calculate the force in the contact elements in which V is a vector representing the relative displacements of the coincident nodes located on the joint surface in the local directions indicating the contact state in various directions so that V_n, the normal relative displacement, indicates the open and/or closed state of the joint. V_r and V_s indicate the state of the considered contact element in tangential directions (Azmi and Paultre, 2002). Moreover, Fig. 2 depicts the force deflection relations for both the normal and the tangential status. In this flowchart, F_n, F_r, and F_s are the local components of the force vector, F_g is the sliding force in the joint, F_t is the shear force resultant in the joint, K_n and K_t are the normal and tangential stiffness of the joint, respectively, and α is the angle between the two

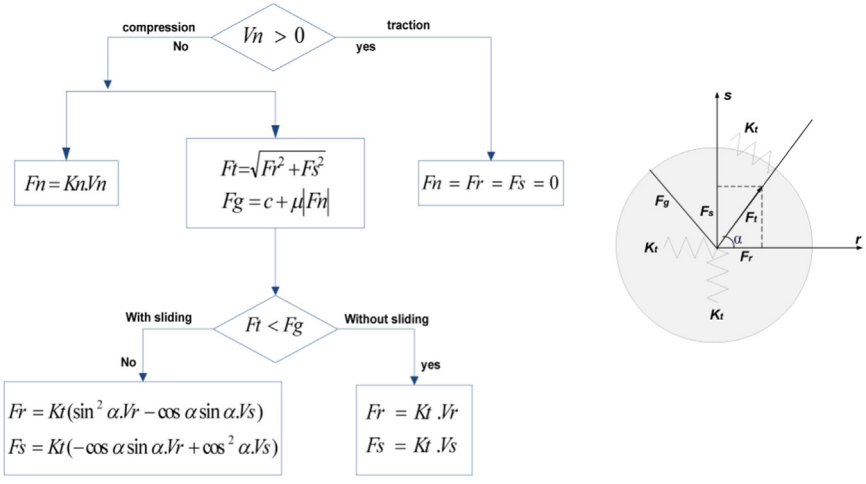

Fig. 1. Flowchart for calculating forces in joints (Hariri-Ardebili and Mirzabozorg, 2012).

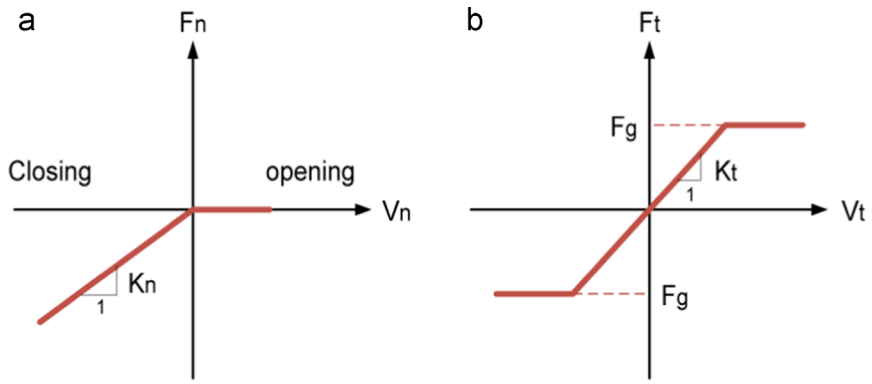

Fig. 2. Force–deflection relations for joint: (a) normal opening; (b) tangential movement (Hariri-Ardebili and Mirzabozorg, 2012).

components of the in-plane shear (Hariri-Ardebili and Mirzabozorg, 2012).

It should be noted that F_g in Fig. 2(b) is equal to F_n multiplied by the friction coefficient. As shown, the contact element cannot endure any tensile force or stress. However, when it is in compression, it can suffer compression forces according to its normal stiffness and shear forces according to its tangential stiffness. When the resultant shear force in the joint exceeds the joint sliding resisting force, the two nodes of the element begin sliding with respect to each other. The joint sliding force is calculated using the Coulomb friction law. In Fig. 1, c is the cohesion factor and μ is the friction coefficient. In concrete dams, the cohesion factor is usually assumed to be zero because of its negligible effect on the results. Also, the friction coefficient is assumed to be unity so that the friction angle is 45°.

4. Constitutive law for mass concrete

In the present paper, material nonlinearity is modeled utilizing the smeared crack approach. After the initiation of the fracture process, determined by suitable criteria, the pre-cracked material stress–strain relation is replaced by an orthotropic relation with the material reference axis system aligned with the fracture direction. The stiffness across the cracking/crushing plane is eliminated suddenly or a gradual stress-release criterion is applied. Thus, only the constitutive relation is updated with the propagation of cracks and the finite element mesh remains unchanged.

In the model, it is assumed that concrete material is initially isotropic and linear until it reaches the predefined criteria. Then, the modulus matrix of concrete is replaced by a modulus matrix evaluated based on the fracture directions. For instance, in a one-dimensional space, the updated secant modulus, E_s, is used instead of the linear initial, E, based on the principal strain reached in the current step. The plasticity-based five-parameter Willam–Warnke model is utilized to model the failure surface (Willam and Warnke, 1975). Both cracking and crushing failure modes are taken into account so that the criterion for failure of the concrete, due to a multi-axial stress state, is satisfied (ANSYS, 2007).

In the model, the presence of a crack at a Gaussian point and in a specified direction is represented by the modification of the modulus matrix and by the introduction of the shear transfer coefficient, β_t, in the cracked plane. The typical shear transfer coefficient ranges from 0.0 to 1.0, with 0.0 representing a smooth crack (complete loss of shear transfer) and 1.0 representing a rough crack (no loss of shear transfer). This specification may be made whether the crack is closed or open (ANSYS, 2007). β_t is the open shear transfer coefficient and defined as the factor that represents the shear strength reduction across the cracked face. In fact, shear transfer coefficients make the shear stiffness entities in the modulus matrix of the cracked Gaussian point. In the present study, the value for parameter β_t is taken to be 0.2. Fig. 3 illustrates the stress–strain curve utilized to model the mass concrete behavior during elastic and softening phases (Hariri-Ardebili and Mirzabozorg, 2012). In this figure, f_t is the cracking stress, ε^{ck} is the strain corresponding to the stress at the level of tensile strength, T_c is the reduction coefficient of tensile stress taken to be 0.6 in the current study, and E_s is the secant modulus of elasticity. In the model utilized for tension, it has been assumed that the fracture strain of concrete is 6 times that corresponding to the softening initiation, as shown in Fig. 3 and pointed out by Taylor et al. (1976).

If the crack is closed, all compressive stresses orthogonal to the crack plane can be transmitted. Only shear transfer coefficient β_c is applied to the modulus matrix to reduce the shear strength relative to the un-cracked case. The value of this parameter in the present study is taken to be 0.9 based on the first author's previous works, such as Hariri-Ardebili et al. (2013c). At last, when a Gaussian point meets the crushing criterion, its contribution to the modulus matrix is disregarded. Some important details on the formulation for simulating the cracking/crushing in mass concrete, corresponding to the utilized failure surfaces and the relevant constitutive law, can be found in Appendix A.

Finally, the modulus matrix is transferred to the element coordinate system by the transform matrix $[T^{ck}]$ as

$$[D_c] = [T^{ck}]^T [D_c^{ck}][T^{ck}] \tag{12}$$

in which $[D_c^{ck}]$ is the modulus matrix of the cracked element aligned to the principal strains and $[D_c]$ is the matrix aligned in

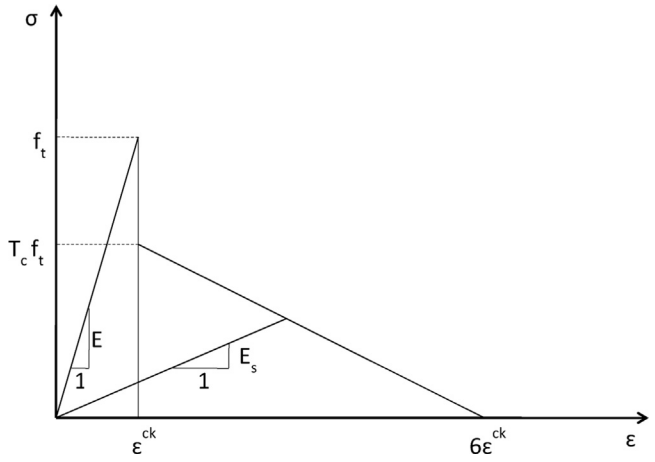

Fig. 3. Stress–strain curvature of mass concrete in tension (Hariri-Ardebili and Mirzabozorg, 2012).

the global directions. The above-mentioned transform matrix is a function of the directions of principal strains and this is the reason that the utilized smeared crack approach is known as the rotating crack approach in which the modulus matrix is aligned with the principal directions in each step of the analysis. It should be noted that if a Gaussian point is fractured in the uniaxial, bi-axial or tri-axial case, the mass concrete is considered as crushed. Hence, the crushed element is completely eliminated from the stiffness matrix and its force is allocated to the adjacent elements.

5. Formulation and solution technique

5.1. Fluid–structure-interaction

Considering the coupled dam–reservoir–foundation system, the governing equation for the reservoir medium is the Helmholtz equation, namely,

$$\nabla^2 p = \frac{1}{C^2}\frac{\partial^2 p}{\partial t^2} \tag{13}$$

where p, C, and t are the hydrodynamic pressure, the pressure wave velocity in the liquid domain, and time, respectively. The partial absorptive boundary is applied on the reservoir and the Sommerfeld boundary is applied on the far-end of the truncated reservoir. Other boundary conditions, applied to the reservoir medium to solve Eq. (13), can be found in Mirzabozorg and Ghaemian (2005) and Mirzabozorg et al. (2003b). The governing equation for the structure and the reservoir take the following form:

$$\begin{bmatrix} [M] & 0 \\ \rho[Q]^T & [G] \end{bmatrix}\begin{Bmatrix} \ddot{U} \\ \ddot{P} \end{Bmatrix} + \begin{bmatrix} [C] & 0 \\ 0 & [C'] \end{bmatrix}\begin{Bmatrix} \dot{U} \\ \dot{P} \end{Bmatrix} + \begin{bmatrix} [K] & -[Q] \\ 0 & [K'] \end{bmatrix}$$

$$\begin{Bmatrix} U \\ P \end{Bmatrix} = \begin{Bmatrix} \{f_1\} - [M]\{\ddot{U}_g\} \\ \{F\} - \rho[Q]^T\{\ddot{U}_g\} \end{Bmatrix} \tag{14}$$

where $[M]$, $[C]$, and $[K]$ are the mass, damping, and stiffness matrices of the structure, respectively, including the dam body and its surrounding foundation rock, and $[G]$, $[C']$, and $[K']$ are the matrices representing the mass, damping, and stiffness equivalent matrices of the reservoir, respectively. Matrix $[Q]$ is the coupling matrix, $\{f_1\}$ is the force vector including both body and hydrostatic force, $\{P\}$ and $\{U\}$ are the vectors of hydrodynamic pressures and displacements, respectively, and $\{\ddot{U}_g\}$ is the ground acceleration vector. $\{F\}$ is the force vector due to integration on all the reservoir boundaries. $\{\dot{P}\}$ and $\{\ddot{P}\}$ are the first and second time derivatives of the nodal hydrodynamic pressure vector, respectively, and ρ is the water density.

A quasi-elastic damping model is utilized in which the cracked elements contribute to the damping matrix with their updated stiffness. The stiffness and mass proportional damping, equivalent to 10% of the critical damping based on the 2 Hz and 6 Hz frequencies of the dam–foundation system, are applied to the structure and the related proportional coefficients are determined as proposed by Hall (2006).

5.2. Numerical solution

In the present paper, the Newton–Raphson method is used to update the model stiffness. Newton–Raphson equilibrium iterations provide convergence at the end of each load increment within the defined tolerance limits. Prior to each solution, the Newton-Raphson approach assesses the out-of-balance load vector, which is the difference between the restoring forces (the loads corresponding to the element stresses) and the applied loads. Subsequently, the program carries out a linear solution using the out-of-balance loads and checks for convergence. If convergence criteria are not satisfied, the out-of-balance load vector is reevaluated, the stiffness matrix is updated, and a new solution is attained. This iterative procedure continues until the problem converges. In this study, the convergence criteria are based on force and displacement for the solid elements with concrete material, and the convergence criteria are based on pressure for the reservoir fluid elements. For dynamic analyses, the Newmark-β method is utilized for the direct integration of Eq. (14) along the subsequent time steps.

6. Finite element model

Dez is a 203-m-high double curvature arch dam with a perimetral joint separating the dam body from a concrete saddle structure called Pulvino. The dam is located in a narrow gorge on the Dez River in the Khuzestan Province in Iran. It is about 150 km north of the provincial capital of Ahwaz. The thickness of the dam at the crest is 4.5 m and its maximum thickness at the base is 21 m. The finite element model is presented in Fig. 4. The dam, surrounding rock, and water are prepared with ANSYS software (ANSYS, 2007).

In arch dams, the dimensions of the foundation are usually considered as being at least twice as much as the dam height (consistent with topography of the site) to diminish the effects of the far-end boundary conditions on the response. This is a general comment and has been mentioned in several guidelines, such as FERC (1999) and USACE (1994), (2007). The model

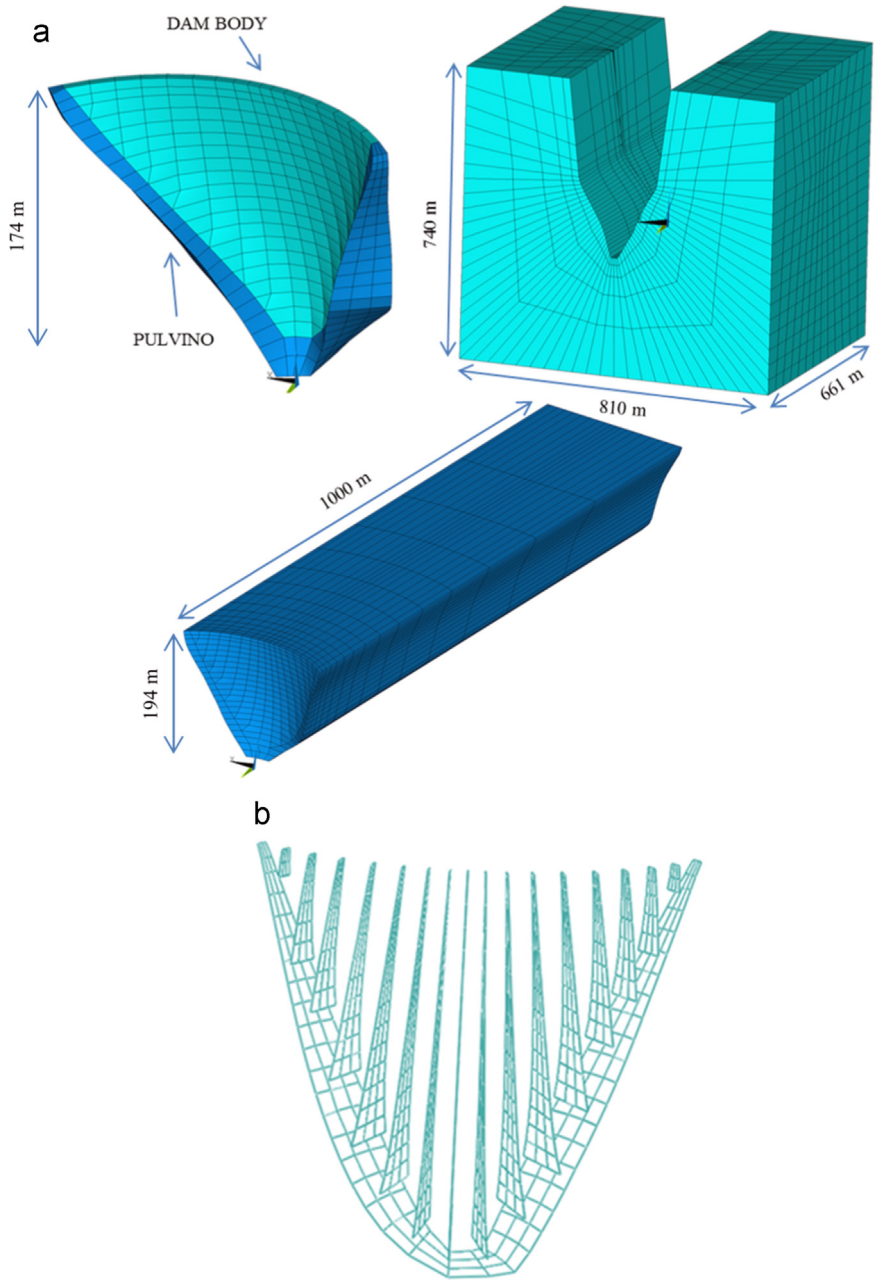

Fig. 4. Finite element model: (a) dam-reservoir-foundation system; (b) contraction and perimetral joints (Hariri-Ardebili and Mirzabozorg, 2012).

consists of 792 8-node solid elements, to model the concrete dam and its saddle, and 3770 8-node solid elements, to model the surrounding foundation rock. The 8-node solid elements have three translational degrees of freedom at each node. In addition, water is modeled using 3660 8-node fluid elements having three translational DOFs and one pressure DOF in each node. It should be noted that translational DOFs are active only at nodes that are on the interface with solid elements. In addition, 956 contact elements are used to model the contraction and perimetral joints. The material properties for the mass concrete and the foundation are described in Table 1 (Hariri-Ardebili et al., 2011).

Normal and tangential stiffness for the contact elements are taken as 240 GPa/m and 24 GPa/m, respectively, extracted from sensitivity analyses conducted by the first author in his previous works. These stiffness coefficients lead to the reasonable opening/closing/sliding of the contraction joints in comparison with the results obtained from joint meters installed in the central block of the dam (Hariri-Ardebili et al., 2011). The water density and sound velocity of the reservoir are taken as 1000 kg/m^3 and 1440 m/s, respectively. The wave reflection coefficient for the reservoir around the boundary is conservatively assumed to be 0.8. It is worth noting that the calibration and validity of the FE model under thermal, self-weight, and hydrostatic loads was previously considered by the first author and his co-workers by comparing the results obtained from the model with those calculated during the monitoring procedure of the dam body as reported in Hariri-Ardebili et al. (2011).

Generally, the seismic performance evaluation of arch dams is considered during a maximum credible earthquake (MCE). Based on the seismic hazard analysis of the dam site (Behansad Engineering and Consulting Co., 2009), the design spectrum of the horizontal and vertical components for the MCE level were extracted considering $\xi=5\%$. The Manjil ground motion is selected for the analysis of the dam based on source characteristics, source-to-site transmission path properties, site conditions, and a scaled record using the design response spectra developed for the dam site (see Fig. 5). The horizontal and vertical PGA's for the scaled record at MCE are 0.43 g, and 0.33 g, respectively.

It should be mentioned that this earthquake is the governing one based on the results obtained from the conducted analyses; and therefore, the results corresponding to this earthquake are represented herein. All three components are applied simultaneously to the investigated model at the dam foundation interface as the free field excitation; and therefore, there is no change in the input due to the damping characteristics of the surrounding rock. In addition, the effect of spatially varying the ground motion is not considered in the current investigation. It is worth noting that the summer loading conditions, which include the reservoir normal water level and the temperature distribution corresponding to that level, are applied to all the conducted analyses before exciting the models using the selected earthquake records.

Table 1
Material properties for mass concrete and foundation rock (Hariri-Ardebili et al., 2011).

Label	Static	Dynamic
$E_{concrete}$ (GPa)	40	46
$\rho_{concrete}$ (kg/m^3)	2400	2400
$\upsilon_{concrete}$	0.20	0.14
$f_t^{concrete}$ (MPa)	3.40	5.10
$f_c^{concrete}$ (MPa)	35.0	36.5
Friction factor (μ)	1	1
Cohesion factor (C)	0	0
E_{rock} (GPa)	13–15	13–15
ρ_{rock} (kg/m^3)	2600	2600
υ_{rock}	0.25	0.25
ρ_{water} (kg/m^3)	1000	1000
C_{water} (m/s)	1440	1440

7. Analyses including joint nonlinearity

In all the analyses, the joint nonlinearity denotes the case in which the material is assumed to be elastic, and the geometric nonlinearity due to the opening/sliding of the contraction vertical and peripheral joints is modeled by the contact elements. Also, the joint and material nonlinearity denotes the case in which the joints are modeled, and the nonlinear behavior of the mass concrete in a 3D space is modeled using a co-axial rotating smeared crack approach. In this section, a nonlinear analysis, including joint nonlinearity, is conducted assuming two types of foundations: (1) where the foundation mass is disregarded (2) where the massed foundation is considered and the viscous boundary is on the far-end truncated boundary of the foundation rock. Fig. 6 presents the non-concurrent envelope of the first principal stresses (tensile stress) on the upstream and downstream faces for both the massless and the massed foundation models, respectively. It should be noted that the tensile stress is defined as positive in the results. Furthermore, the non-concurrent envelopes for the third principal stress (compressive stress) are presented in Fig. 7. As shown in the plots, the distribution patterns of the stresses are the same for both models, but the massed foundation model leads to much lower stress levels within the dam body. According to the figures, both the intensity and the extension of the tensile overstressed areas are much more evident in the middle part on the downstream face, whereas high compressive stressed regions occur in the upper middle part near the crest cantilever on the upstream face.

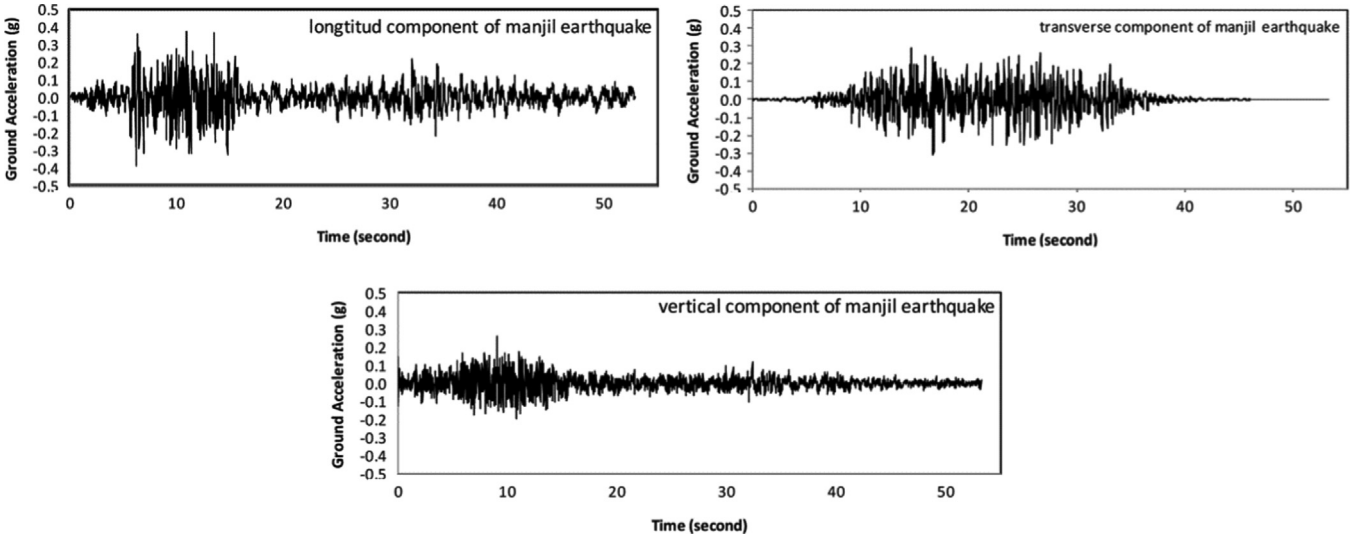

Fig. 5. Manjil ground motion recorded at Abbar station.

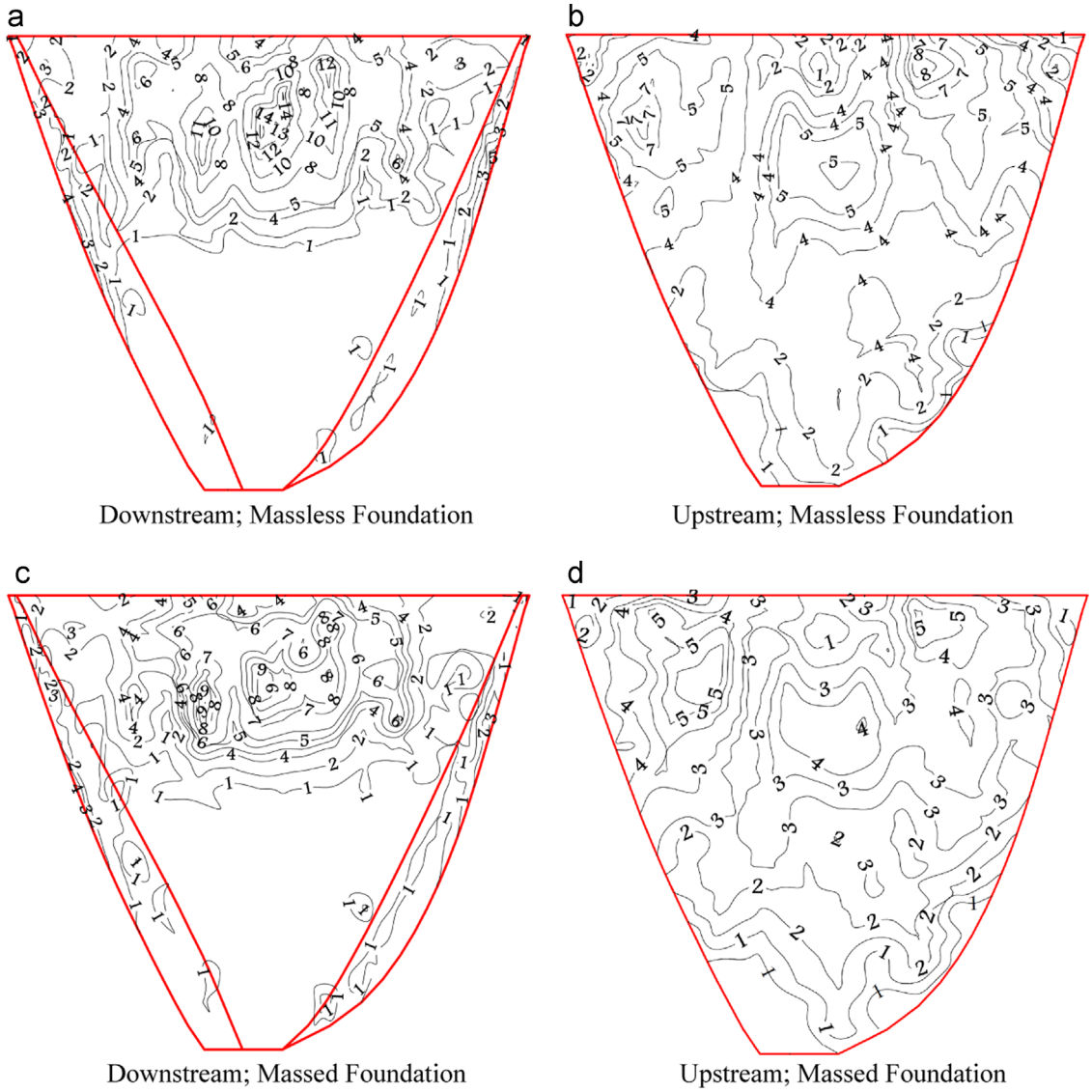

Fig. 6. Non-concurrent envelope of the first principal stress on the upstream and downstream faces for MCE in summer conditions (MPa).

Table 2 presents the maximum tensile and compressive stresses resulting from the conducted analyses. It is worth noting that in Figs. 6–8, the positive and negative values for the line stress contours correspond to tensile and compressive stresses, respectively, and comparing the numbers on each line in Fig. 6 to the tensile strength specified in Table 1, it can be seen that in some areas there are tensile stresses higher than the dynamic tensile strength of the mass concrete. When the system is modeled using a massed foundation, the maximum values for tensile and compressive stresses decreased by 32% and 25%, respectively, in comparison with the case of a massless foundation. Considering foundation flexibility without the effect of mass results in a larger response. This overestimation is due to a decrease in overall damping caused by ignoring the foundation damping-material and radiation and by disregarding the inertia effect of the huge mass in the surrounding rock. Unfortunately, this trend leads to inaccurate conclusions such that existing dams are unsafe and require upgrading.

In order to determine the degree of joint nonlinearity of the system, the results were compared with those obtained from the linear model considering the massed foundation (presented in Fig. 8). Comparing Fig. 8 with Figs. 6 and 7, it is observed that considering the joint nonlinearity leads to higher compressive stresses through the dam body. However, tensile stresses within the dam body are lower than those obtained from the linear analysis.

8. Analysis including joint and material nonlinearities

According to the results of the nonlinear analysis, there are no cracked or crushed Gaussian points due to the self-weight or hydrostatic loads at the first load step. At later stages, the system in both models is excited simultaneously in the three directions using the scaled components of the Manjil Earthquake. Fig. 9 presents the crack/crushed profiles on the upstream and downstream faces when the foundation medium is assumed to be massless, while Fig. 10 depicts the results

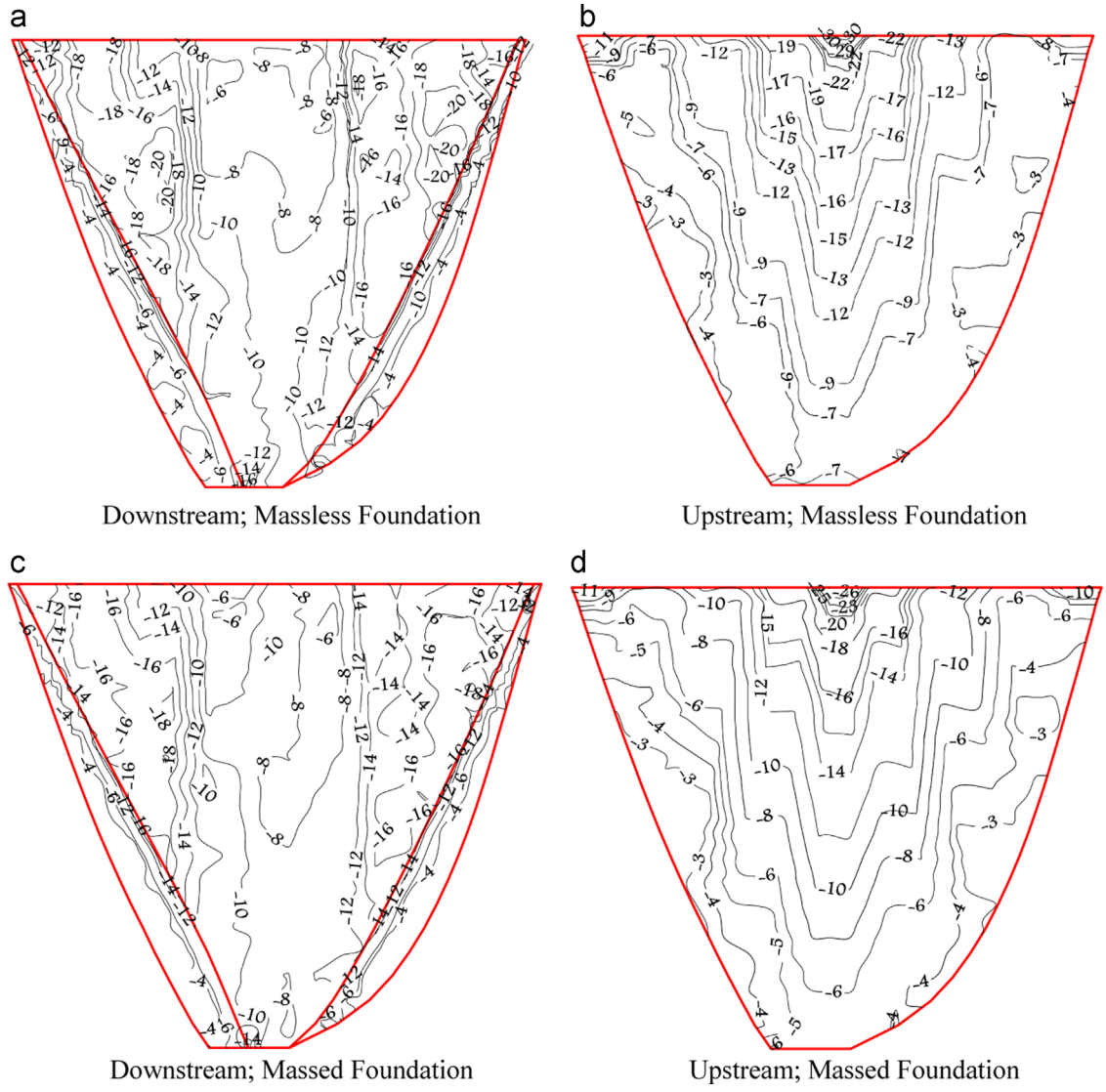

Fig. 7. Non-concurrent envelope of the third principal stress on upstream and downstream faces for MCE in summer conditions (MPa).

Table 2
Maximum values of tensile and compressive stresses within the dam body in MCE.

Stress	Analysis type	Foundation state	Value (MPa)
Compressive	Nonlinear (joint)	Massless	34.6
		Massed	26
	Linear	Massed	22
Tensile	Nonlinear (joint)	Massless	14.6
		Massed	10
	Linear	Massed	12.5

when the massed foundation and the viscous condition on the far-end truncated boundary of the foundation are considered.

In the model with the massless foundation, the analysis is terminated at 12 s due to numerical instability. However, there is no instability in the model including the massed foundation, for which it can be argued that after MCE, sudden abandonment of the water will not occur. Comparing the crack profiles shown in Figs. 9 and 10, the massed foundation model leads to many fewer cracked Gaussian points in comparison to the model with the massless foundation which is a more realistic conclusion. In addition, the upper half of the dam body is cracked in the model with the massless foundation. However, in the model with the massed foundation, only some upper middle parts of the dam body near the crest cantilever are cracked, which is in good agreement with the overstressed areas in their counterpart analysis including joint nonlinearity.

9. Conclusions

In the present paper, the FE model for the Dez dam, an existing high arch dam located in Iran, including a reservoir and foundation, was excited using the three components of the Manjil Earthquake at the dam-foundation interface. The nonlinear behavior of the mass concrete was modeled using a coaxial rotating smeared crack approach in which a well-known five-parameter failure criterion was used as the cracking/

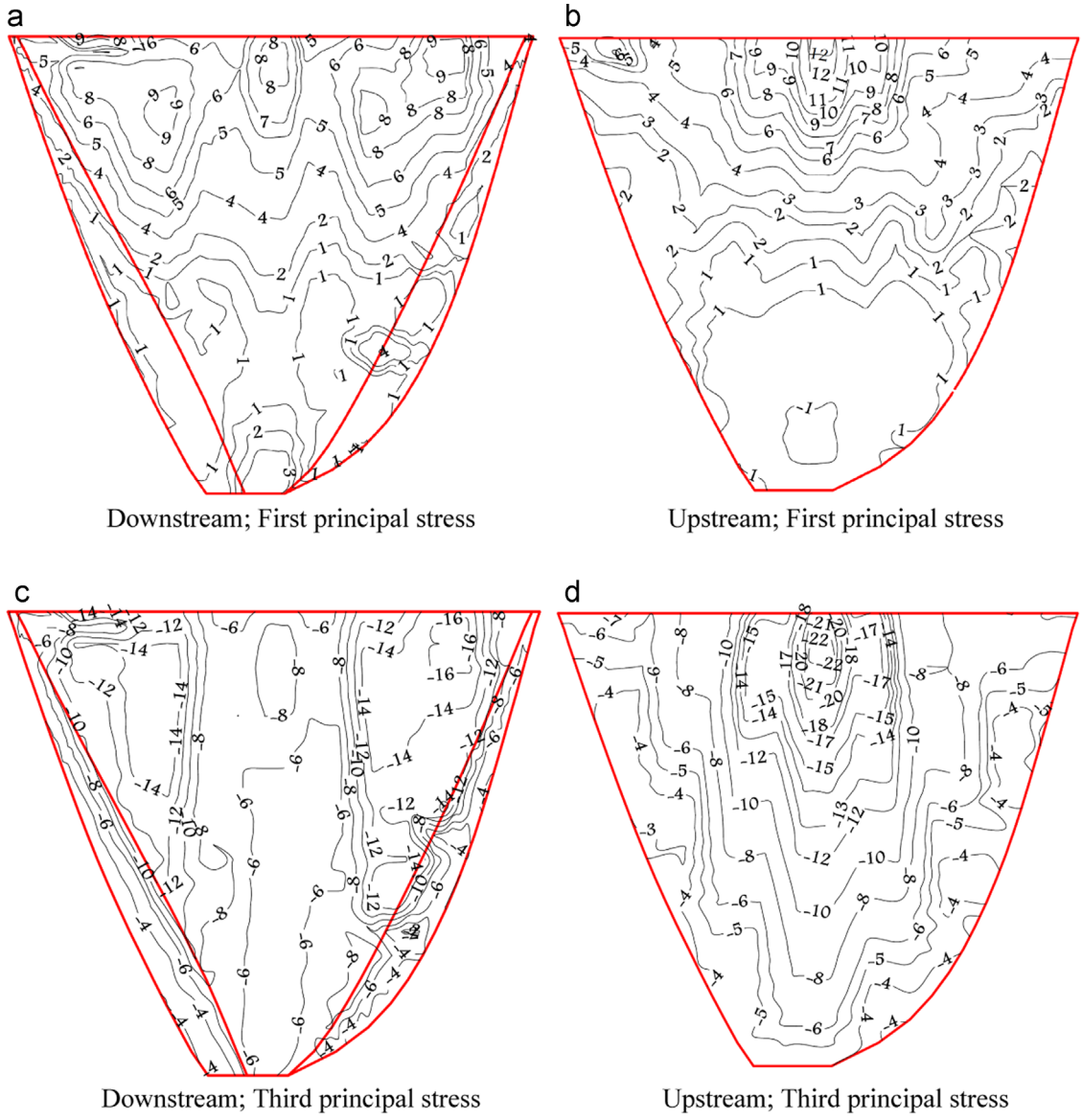

Fig. 8. Non-concurrent envelope of the first and third principal stresses on upstream and downstream faces for MCE in summer conditions (MPa) for the linear model.

crushing initiation criterion. In addition, node-to-node contact elements were used to model the contraction/perimetral joints, as reported in as-built drawings. The Dam–reservoir interaction was accounted for by the finite element method and the reservoir was assumed to be compressible. The two sets of analyses were conducted to consider the effects of the massed foundation on the nonlinear seismic response of the system, the massless foundation model, and the massed foundation model with the viscous dampers on the far-end truncated boundary of the surrounding rock.

Based on the results, it was observed that modeling the foundation as a massless medium leads to the significant overestimation of the response of the system. In the nonlinear analysis, including joint nonlinearity, the maximum tensile and compressive stresses were reduced by 32% and 25%, respectively, when the foundation was assumed to be massed in comparison to the results obtained with the massless foundation model. It was also seen that considering joint nonlinearity leads to higher compressive stresses and lower tensile stresses than those obtained from the linear analysis. In fact, the contraction joints release tensile arch stresses on the upstream face, leading to the redistribution of the stresses within the dam body and changes in the arch performance of the body to the cantilever one in compression. This phenomenon leads to more values of compressive stresses, which is the expected behavior in arch concrete dams.

In the nonlinear analyses, including both joint and material nonlinearities, modeling the foundation as a massed medium led to many fewer cracked Gaussian points within the dam body, which is an important phenomenon in a seismic safety assessment of existing dams. In addition, in the model with the massless foundation, the upper half of the dam body was cracked, while in the model including the massed foundation, cracking occurred only in upper middle parts near the crest

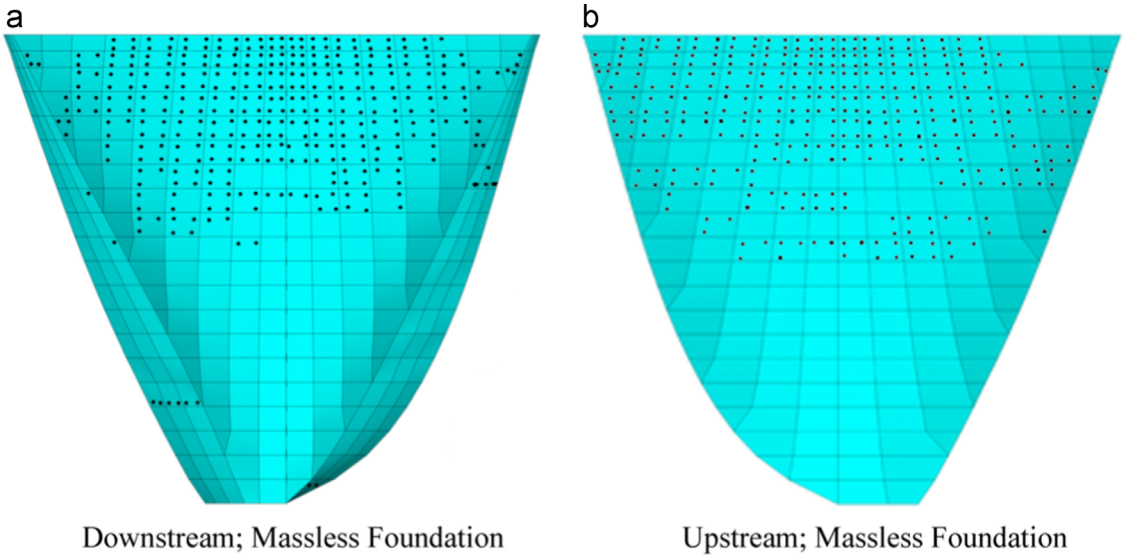

Fig. 9. Cracking within the dam body for massless foundation.

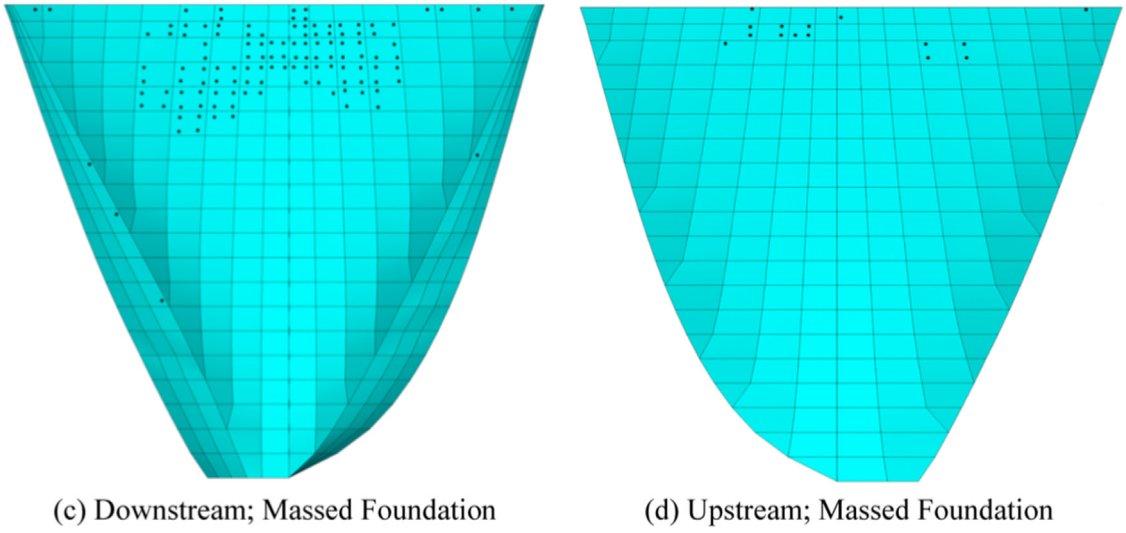

Fig. 10. Cracking within the dam body for massed foundation.

cantilever, which was in good agreement with the overstressed areas in their counterpart analyses including joint nonlinearity. In addition, there was no instability in the model with the massed foundation, for which it can be argued that the dam body is safe in MCE. However, to achieve more realistic results, other factors such as the spatial variation in ground motion, should be considered.

Appendix A. Five-parameter Willam–Warnke model

In the current study, the plasticity-based five-parameter Willam–Warnke model (1975) is utilized as the failure criterion in mass concrete (ANSYS, 2007). The failure criterion of concrete due to a multi-axial stress state can be expressed in the following form:

$$\frac{\Omega}{f_c} - \gamma \geq 0 \tag{A.1}$$

where Ω is a function of the principal stress state, f_c is the compressive strength of concrete, and γ is the failure surface expressed in terms of principal stresses and the five input parameters defined in Table 3. If Eq. (A.1) is satisfied, cracking or crushing of the concrete occurs. Whenever one of the principal stresses is tensile, cracking occurs, and when all principal stresses are compressive, crushing occurs. The failure surface is specified with two parameters, f_c and f_t, and the other parameters are calculated with the Willam–Warnke model by default as (ANSYS, 2007)

$$f_{cb} = 1.2 f_c$$

Table 3
Concrete material table (ANSYS, 2007).

Label	Description
f_t	Ultimate uniaxial tensile strength
f_c	Ultimate uniaxial compressive strength
f_{cb}	Ultimate biaxial compressive strength
σ_h^a	Ambient hydrostatic stress state
f_1	Ultimate compressive strength for a state of biaxial compression superimposed on hydrostatic stress state
f_2	Ultimate compressive strength for a state of uniaxial compression superimposed on hydrostatic stress state

$$f_1 = 1.45 f_c$$
$$f_2 = 1.725 f_c \tag{A.2}$$

These default values are valid only for stress states where the following condition is satisfied:

$$\left|\sigma_h\right| \le \sqrt{3} f_c \tag{A.3}$$

σ_h, which is equal to σ_h^a, is the hydrostatic stress expressed as

$$\sigma_h = \frac{1}{3}(\sigma_{xp} + \sigma_{yp} + \sigma_{zp}) \tag{A.4}$$

Both function Ω and failure surface γ are expressed in terms of principal stresses denoted as σ_1, σ_2, and σ_3 as

$$\sigma_1 = \max(\sigma_{xp}, \sigma_{yp}, \sigma_{zp})$$
$$\sigma_3 = \min(\sigma_{xp}, \sigma_{yp}, \sigma_{zp}) \tag{A.5}$$

so that, $\sigma_1 \ge \sigma_2 \ge \sigma_3$

The failure of concrete is categorized into the following four domains:

1. $0 \ge \sigma_1 \ge \sigma_2 \ge \sigma_3$ means compression – compression – compression state
2. $\sigma_1 \ge 0 \ge \sigma_2 \ge \sigma_3$ means tensile – compression – compression state
3. $\sigma_1 \ge \sigma_2 \ge 0 \ge \sigma_3$ means tensile – tensile – compression state
4. $\sigma_1 \ge \sigma_2 \ge \sigma_3 \ge 0$ means tensile – tensile – tensile state

The general function, Ω, and the failure surface, γ, can be divided into four independent sub-functions in each domain, which can be found in ANSYS, (2007). Parameters f_1, f_2, f_{cb}, and σ_h^a are used to form the desired stress functions and failure surfaces in the above-mentioned domains (see ANSYS, 2007).

In order to apply the above-mentioned constitutive law, it is assumed that concrete material is initially (before cracking/crushing) isotropic and linear. The stress–strain matrix is defined by (A.6) as

$$[D_{linear}.] = \frac{E}{(1+\nu)(1-2\nu)} \begin{bmatrix} (1-\nu) & \nu & \nu & 0 & 0 & 0 \\ \nu & (1-\nu) & \nu & 0 & 0 & 0 \\ \nu & \nu & (1-\nu) & 0 & 0 & 0 \\ 0 & 0 & 0 & \frac{1-2\nu}{2} & 0 & 0 \\ 0 & 0 & 0 & 0 & \frac{1-2\nu}{2} & 0 \\ 0 & 0 & 0 & 0 & 0 & \frac{1-2\nu}{2} \end{bmatrix} \tag{A.6}$$

where E is the initial isotropic Young's modulus for concrete and ν is Poisson's ratio. Cracking occurs in concrete when the principal tensile stress in any direction lies outside the failure surface. When cracking occurs at an integration point, the stress–strain relation is replaced by defining a weak plane normal to the crack direction, which is unable to endure any tensile stress.

Based on the fact that concrete can be cracked in one, two or three orthogonal directions, the modulus matrix can be represented in the following forms:

I) Concrete is cracked in one direction and the crack is open

$$[D_c^{ck}] = \frac{E}{1+\nu} \begin{bmatrix} \frac{E_s(1+\nu)}{E} & 0 & 0 & 0 & 0 & 0 \\ 0 & \frac{1}{1-\nu} & \frac{\nu}{1-\nu} & 0 & 0 & 0 \\ 0 & \frac{\nu}{1-\nu} & \frac{1}{1-\nu} & 0 & 0 & 0 \\ 0 & 0 & 0 & \frac{\beta_t}{2} & 0 & 0 \\ 0 & 0 & 0 & 0 & \frac{1}{2} & 0 \\ 0 & 0 & 0 & 0 & 0 & \frac{\beta_t}{2} \end{bmatrix} \tag{A.7}$$

where E_s is the secant modulus of elasticity.

II) Concrete is cracked in one direction and the crack is closed

$$[D_c^{ck}] = \frac{E}{(1+\nu)(1-2\nu)} \begin{bmatrix} (1-\nu) & \nu & \nu & 0 & 0 & 0 \\ \nu & (1-\nu) & \nu & 0 & 0 & 0 \\ \nu & \nu & (1-\nu) & 0 & 0 & 0 \\ 0 & 0 & 0 & \frac{\beta_c(1-2\nu)}{2} & 0 & 0 \\ 0 & 0 & 0 & 0 & \frac{1-2\nu}{2} & 0 \\ 0 & 0 & 0 & 0 & 0 & \frac{\beta_c(1-2\nu)}{2} \end{bmatrix} \tag{A.8}$$

III) Concrete is cracked in two directions and the cracks are open:

$$[D_c^{ck}] = E \begin{bmatrix} \frac{E_s}{E} & 0 & 0 & 0 & 0 & 0 \\ 0 & \frac{E_s}{E} & 0 & 0 & 0 & 0 \\ 0 & 0 & 1 & 0 & 0 & 0 \\ 0 & 0 & 0 & \frac{\beta_t}{2(1+\nu)} & 0 & 0 \\ 0 & 0 & 0 & 0 & \frac{\beta_t}{1(1+\nu)} & 0 \\ 0 & 0 & 0 & 0 & 0 & \frac{\beta_t}{2(1+\nu)} \end{bmatrix} \tag{A.9}$$

IV) Concrete is cracked in two directions and both cracks are closed:

$$\left[D_c^{ck}\right]=\frac{E}{(1+\nu)(1-2\nu)}\begin{bmatrix}(1-\nu) & \nu & \nu & 0 & 0 & 0\\ \nu & (1-\nu) & \nu & 0 & 0 & 0\\ \nu & \nu & (1-\nu) & 0 & 0 & 0\\ 0 & 0 & 0 & \frac{\beta_c(1-2\nu)}{2} & 0 & 0\\ 0 & 0 & 0 & 0 & \frac{(1-2\nu)}{2} & 0\\ 0 & 0 & 0 & 0 & 0 & \frac{\beta_c(1-2\nu)}{2}\end{bmatrix} \tag{A.10}$$

V) Concrete is cracked in three directions and the cracks are open:

$$\left[D_c^{ck}\right]=E\begin{bmatrix}\frac{E_s}{E} & 0 & 0 & 0 & 0 & 0\\ 0 & \frac{E_s}{E} & 0 & 0 & 0 & 0\\ 0 & 0 & 1 & 0 & 0 & 0\\ 0 & 0 & 0 & \frac{\beta_t}{2(1+\nu)} & 0 & 0\\ 0 & 0 & 0 & 0 & \frac{\beta_t}{2(1+\nu)} & 0\\ 0 & 0 & 0 & 0 & 0 & \frac{\beta_t}{2(1+\nu)}\end{bmatrix} \tag{A.11}$$

VI) Concrete is cracked in three directions and all cracks are closed. In this situation, (A.10) can be written again. It must be noted that all the above stress–strain relations are written in a local coordinate system that is parallel to the principal strain directions.

If a Gaussian point meets the failure criterion in compression, its contribution to the stiffness matrix is disregarded.

References

Alves, S.W., 2004. Nonlinear Analysis of Pacoima Dam with Spatially Uniform Ground Motion. California Institute of Technology, Pasadena, CA.

ANSYS, 2007. ANSYS version 11.0.1 reference manual. ANSYS Inc., Canonsburg, PA.

Azmi, M., Paultre, P., 2002. Three-dimensional analysis of concrete dams including contraction joint nonlinearity. Eng. Struct. 24 (6), 757–771.

Behan-sad Engineering and Consulting Co., 2009. Seismic hazard analysis of DEZ dam, Tehran, Iran.

Berrabah, A.T., Armouti, N., Belharizi, M., Bekkouchi, A., 2012. Dynamic soil structure interaction study. Jourdan J. Civ. Eng. 6 (2), 161–173.

Chopra, A.K., 2012. Earthquake analysis of arch dams: factors to be considered. ASCE J. Struct. Eng. 138 (2), 205–214.

FERC, 1999. Engineering guidelines for the evaluation of hydropower projects: Chapter 11-Arch dams. Federal Energy Regulatory Commission, Washington D.C.

Fok, K.L., Hall, J.F., Chopra, A.K., 1986. EACD-3D: A Computer Program for Three-Dimensional Earthquake Analysis of Concrete Dams, Report No. UCB/EERC-86/09. University of California Berkeley, CA. ⟨http://nisee.berkeley.edu/documents/EERC/EERC-86-09.pdf⟩.

Ghaemian, M., Noorzad, A., Moghaddam, R.M., 2005. Foundation effect on seismic response of concrete arch dams including dam-reservoir interaction. Int. J. Earthq. Eng. Eng. Seismol. (EEE) 3, 49–57.

Hall, J.F., 1998. Efficient non-linear seismic analysis of arch dams. Earthq. Eng. Struct. Dyn. 27 (12), 1425–1444.

Hall, J.F., 2006. Problems encountered from the use (or misuse) of Rayleigh damping. Earthq. Eng. Struct. Dyn. 35 (5), 525–545.

Hariri-Ardebili, M.A., Mirzabozorg, H., Ghaemian, M., Akhavan, A., Amini, R., 2011. Calibration of 3D FE model of DEZ high arch dam in thermal and static conditions using instruments and site observation. In: Proceedings of the Sixth International Conference in Dam Engineering. Lisbon, Portugal.

Hariri-Ardebili, M.A., Mirzabozorg, H., 2012. Seismic performance evaluation and analysis of major arch dams considering material and joint nonlinearity effects. Int. Sch. Res. Netw. Civ. Eng. 2012, 1–10 . http://dx.doi.org/10.5402/2012/681350.

Hariri-Ardebili, M.A., Mirzabozorg, H., 2013a. A comparative study of seismic stability of coupled arch dam-foundation-reservoir systems using infinite elements and viscous boundary models. Int. J. Struct. Stab. Dyn. 13 (6), 1350032. http://dx.doi.org/10.1142/S0219455413500326.

Hariri-Ardebili, M.A., Saouma, V., 2013b. Impact of near-fault vs. far-field ground motions on the seismic response of an arch dam with respect to foundation type. Dam Eng. 24 (1), 19–52.

Hariri-Ardebili, M.A., Seyyed-Kolbadi, S.M., Mirzabozorg, H., 2013c. A smeared crack model for seismic failure analysis of concrete gravity dams considering fracture energy effects. Struct. Eng. Mech. 48 (1), 17–39.

Lau, D., Noruziaan, B., Razaqpur, A.G., 1998. Modelling of contraction joint and shear sliding effects on earthquake response of arch dams. Earthq. Eng. Struct. Dyn. 27 (10), 1013–1029.

Lysmer, J., Kuhlemeyer, R.L., 1969. Finite dynamic model for infinite media. J. Eng. Mech. Div., 95; 859–877.

Mirzabozorg, H., Ghaemian, M., 2005. Nonlinear behavior of mass concrete in three-dimensional problems using smeared crack approach. Earthq. Eng. Struct. Dyn. 34 (3), 247–269.

Mirzabozorg, H., Ghannad, M.A., Ghaemian, M., 2003a. Foundation interaction effect on the seismic response of Amir–Kabir arch dam. In: Proceedings of the Fourth International Conference on Earthquake Engineering and Seismology. Tehran, Iran.

Mirzabozorg, H., Khaloo, A.R., Ghaemian, M., 2003b. Staggered solution scheme for three-dimensional analysis of dam-reservoir interaction. Dam Eng. J. 14 (3), 147–164.

Mirzabozorg, H., Khaloo, A.R., Ghaemian, M., Jalalzadeh, B., 2007. Non-uniform cracking in smeared crack approach for seismic analysis of concrete dams in 3D space. Int. J. Earthq. Eng. Eng. Seismol. (EEE) 2, 48–57.

Mirzabozorg, H., Kordzadeh, A., Hariri-Ardebili, M.A., 2012. Seismic response of concrete arch dams including dam-reservoir-foundation interaction using infinite elements. Electron. J. Struct. Eng. 12 (1), 63–73.

Mirzabozorg, H., Varmazyari, M., Ghaemian, M., 2010. Dam-reservoir-massed foundation system and travelling wave along reservoir bottom. Soil Dyn. Earthq. Eng. 30 (8), 746–756.

Mirzabozorg, H., Varmazyari, M., Noorzad, A., 2010. Non-linear seismic behavior of concrete gravity dams and travelling wave effect along reservoir bottom. Dam Eng. J. 21 (1), 20.

Mojtahedi, S.B., Fenves, G., 2000. Effect of Contraction Joint Opening on Pacoima Dam in the 1994 Northridge Earthquake. University of California, Berkeley, CA.

Noorzad, A., Ghaemian, M., Mirzabozorg, A., 2007. Influence of dam reservoir foundation interaction on the safety evaluation of concrete arch dams. In: Proceedings of the ICOLD 75th Annual Meeting: Focus on Dam Development and Safety. St. Petersburg Russia.

Sevim, B., Altunisik, A.C., Bayraktar, A., 2012. Earthquake behavior of Berke arch dam using ambient vibration test results. J. Perform. Constr. Facil., 26; 780–792.

Tan, H., Chopra, A.K. 1996. EACD-3D-96: a Computer Program for Three-Dimensional Earthquake Analysis of Concrete Dams, Report No. UCB/SEMM-96/06). University of California, Berkeley, CA. ⟨http://nisee.berkeley.edu/documents/SEMM/SEMM-96-06.pdf⟩.

Taylor, R.L., Beresford, P.J., Wilson, E.L., 1976. A non-conforming element for stress analysis. Int. J. Numer. Methods Eng. 10 (6), 1211–1219.

USACE, 1994. Engineering and design: arch dam design, Report No: EM 1110-2-2201. United States Army Corps of Engineers, Washington, D.C.

USACE, 2003. Time-History Dynamic Analysis of Concrete Hydraulic Structures, Report No. EM 11102-6051, United States Army Corps of Engineers Washington, D.C.

USACE, 2007. Earthquake Design and Evaluation of Concrete Hydraulic Structures, Report No: EM 1110-2-6053. United States Army Corps of Engineers, Washington, D.C.

USBR, 1998. Linear Elastic Dynamic Structural Analysis Including Mass in the Foundation for Hoover Dam, Technical Memorandum HVD-MDA-D8110-D8197. United States Bureau of Reclamation, Denver, CO.

USBR, 2002. Static and Dynamic Linear Elastic Structural Analysis, (EACD3D96). Morrow Point Dam, United States Bureau of Reclamation, Denver, CO.

Wang, J.T., Chopra, A.K., 2008. EACD-3D-2008: A Computer Program for Three-dimensional Earthquake Analysis of Concrete Dams Considering Spatial-varying Ground Motion, Report No. UCB/EERC-2008-04. Earthquake Engineering Research Center, University of California Berkeley, CA. ⟨http://nisee.berkeley.edu/documents/EERC/EERC-08-04.pdf⟩.

Wang, J.T., Zhang, C.H., Jin, F., 2012. Nonlinear earthquake analysis of high arch dam–water–foundation rock systems. Earthq. Eng. Struct. Dyn. 41 (7), 1157–1176.

Willam, K.J., Warnke, E.D., 1975. Constitutive model for the triaxial behavior of concrete. In: Proceedings of the International Association for Bridge and Structural Engineering. Vol. 19, ISMES, Bergamo, Italy, p. 174.